International Journal of Impact Engineering 36 (2009) 875–887

Contents lists available at ScienceDirect

International Journal of Impact Engineering

journal homepage: www.elsevier.com/locate/ijimpeng

On the resistance to penetration of stiffened plates, Part II: Numerical analysis

Hagbart S. Alsos [a,*], Jørgen Amdahl [a], Odd S. Hopperstad [b]

[a] Department of Marine Technology, Norwegian University of Science and Technology, Otto Nielsens V. 10, 7491 Trondheim, Norway
[b] Structural Impact Laboratory (SIMLab); Center for Research-based Innovation; Department of Structural Engineering; Norwegian University of Science and Technology, Richard Birkelandsv. 1a, 7491 Trondheim, Norway

ARTICLE INFO

Article history:
Received 1 September 2008
Received in revised form
1 September 2008
Accepted 6 November 2008
Available online 21 November 2008

Keywords:
Plate
Finite element analysis
Fracture
Penetration
Experiment

ABSTRACT

A series of indentation tests have been carried out quasi-statically on various configurations of stiffened panels. These represent hull plates in ships subjected to grounding or collision actions. The results of the scaled down tests are reported in the first part of this two-part companion paper. This part (II) presents results from numerical analyses with focus on fracture prediction.
The performance of two failure criteria is investigated. These are implemented into the explicit finite element code LS-DYNA and are referred to as the BWH instability criterion and the RTCL damage criterion, respectively. In addition, the influence of the element size with respect to onset of failure is studied.
Although the study is aimed towards accidental scenarios considering collision and grounding of ships, the investigation also apply to other types of problems. This may for instance be the response of deck structures which are hit by dropped objects, or the response of stiffened panels subjected to explosions or ice actions.

1. Introduction

Analysis of accidental response of marine structures is more and more performed by means of the finite element method. The rapid increase in computational power allows analysis of large and complex problems. However, problems arise when fracture is included. Presently, there is no practical formulation capable of simulating both fracture initiation and propagation in large-scale structures using shell elements, see for instance Ref. [4]. One reason for this is that fracture most often is modeled by removing over-strained elements. This is an engineering approach which makes FE solutions very mesh sensitive. It also makes modeling of fracture propagation more difficult in the sense that crack tip effects are concentrated over very few elements.

The complexities of determining the onset of fracture were studied in a joint university project dealing with ship collision and grounding, see Ref. [5]. Four commonly used failure criteria were applied in blind fold simulations of actual ship–ship collision tests. The collision experiments were conducted by TNO (the Dutch Institute for Applied Physical Research) and counted four large-scale collision tests [6–8]. In total 36 simulations were carried out. Three collision models were analyzed, each with three different element sizes using the four fracture criteria. The numerical results were compared internally and against the tests. The study showed a significant scatter in the predicted fracture initiation and propagation force, both with respect to results acquired with different mesh sizes and to simulations with the different failure criteria. A lesson learned from the study is that the user's interpretation of the input parameters and how the mesh sensitivity effect is dealt with is equally important as the fracture criterion itself.

Predicting the onset of fracture is especially important in structural members which resist accidental forces by membrane action. This is often the case in ship collision and grounding scenarios. An obstruction, e.g. the sea floor or a ship bow is typically forced into the ship hull. Once the hull is penetrated, the resistance to further indentation typically drops significantly, as reported by Naar et al. [9] and Simonsen and Lauridsen [10]. Of particular concern is penetration of the inner hull and the cargo tanks. This may have severe consequences such as oil spill and flooding of compartments.

In this second part of the two-part article, focus is on predicting fracture in ship collision and grounding scenarios. Two relatively advanced fracture criteria are applied in hull penetration analyses. The assessment is carried out by performing finite element simulations of the quasi-static panel penetration tests presented in Part 1, see Ref. [1].

2. Theoretical aspects – fracture

In most metals alloys, fracture relates to the formation of micro-voids which grow and eventually coalesce during deformation.

* Corresponding author. Tel.: +47 735 50446; fax: +47 735 95697.
E-mail address: hagbarts@ntnu.no (H.S. Alsos).

0734-743X/$ – see front matter © 2008 Elsevier Ltd. All rights reserved.
doi:10.1016/j.ijimpeng.2008.11.004

Such voids form at inclusions or hard second phases in regions which are highly deformed. The growth rate of these voids is controlled by the deformation and the hydrostatic stress state within the material micro structure. Studies on void growth within the microstructure have, for instance, been conducted by McClintock [11] and Rice and Tracey [12]. Eventually, as the voids coalesce and form small cracks, the material reaches a state where fracture is initiated. The importance of the hydrostatic stress state with respect to ductile fracture is investigated further by Hancock and Mackenzie [13], Mackenzie et al. [14] and Bao and Wierzbicki [15–17] who also have paid attention to development of fracture in the shear domain.

The growth of micro-structural flaws and defects is in material modeling often associated with a damage variable D. The evolution of the material damage $\dot{D}$ is a way of describing the rate of void growth and has been used extensively by several authors, e.g. Lemaitre [18], Bonora [19], McClintock [11] and Rice and Tracey [12]. The damage variable may either be coupled to the constitutive material equations or used separately as a local approach to determine the onset of fracture. Applied in a finite element code, the damage approach has proved to be a powerful tool to predict the failure response in deformed material. This, however, implies a detailed mesh, and for many damage models, several material parameters.

In ship crashworthiness analysis the available material data is usually limited. Often the classification society only sets a lower requirement to the steel quality used in ships. Furthermore, the sheer size of ships often results in analyses with coarsely meshed finite element models. This is generally not compatible with a complex damage model. More pragmatic approaches are needed. Predicting onset of fracture based on a critical equivalent plastic strain is a simple and much used criterion. This represents, however, an over-simplification of fracture mechanics, since the influence of the stress state is neglected. An excellent evaluation of applied fracture criteria is given by Wierzbicki et al. [20]. Similarly, Törnqvist [3] presents a summary of fracture criteria applied in analyses of marine accidents.

Two failure criteria are applied in this article. The first one is the so-called Rice–Tracey–Cockcroft–Latham criterion (RTCL) which is presented in detail by Törnqvist [3] and Simonsen and Törnqvist [4]. The second is the Bressan–Williams–Hill (BWH) instability criterion [2]. The criteria are along with material routines implemented into the LS-DYNA finite element software [21]. Both criteria are summarized in the following sections.

2.1. The RTCL damage criterion

The RTCL damage criterion [3] is composed of the modified Cockcroft–Latham–Oh damage criterion [22,23] and the Rice–Tracey damage criterion [12]. Both of these are functions of the hydrostatic stress state, expressed by the stress triaxiality $T = \sigma_m/\sigma_{eq}$. Here σ_m is the hydrostatic stress and σ_{eq} is the equivalent stress. Damage evolution in the shear domain, $-1/3 < T < 1/3$, is represented by the Cockcroft–Latham–Oh damage criterion. An interesting feature with this criterion is that damage evolution ceases when $T < -1/3$. This value is referred to as the cut-off value. It is shown by Bao and Wierzbicki [15] with basis in upsetting tests that fracture will not occur below this value. The Rice and Tracey damage criterion [12] is applied for stress triaxiality levels greater than 1/3, which is often referred to as the void growth domain. An independent evaluation of both the Cockcroft–Latham–Oh damage criterion and the Rice–Tracey criterion is given by Bao and Wierzbicki, see Refs. [16,17], respectively. The RTCL combination of the two damage criteria may be expressed mathematically by the evolution rule

$$\dot{D} = \begin{cases} 0 & \text{if } T < -1/3 \\ \dfrac{\sigma_1}{\sigma_{eq}}\dot{\varepsilon}_{eq} & \text{if } -1/3 \le T < 1/3 \\ \exp\left(\frac{3T-1}{2}\right)\dot{\varepsilon}_{eq} & \text{otherwise} \end{cases} \tag{1}$$

where $\dot{D}$ describes the rate of damage, σ_1 is the major principal stress and $\dot{\varepsilon}_{eq}$ is the rate of the equivalent plastic strain. Fracture is initiated once the accumulated damage reaches a critical level. An important feature with this criterion is that for proportional loading in uniaxial tension ($T = 0.33$), the damage evolution $\dot{D}$ is exactly matched by the rate of equivalent plastic strain $\dot{\varepsilon}_{eq}$. This is convenient with respect to calibration, because the critical damage D_{cr} most easily can be found from uniaxial tensile tests. From this a normalized criterion can be expressed as

$$D = \frac{1}{\varepsilon_{cr}}\int \dot{D}dt \tag{2}$$

where ε_{cr} is the critical equivalent plastic strain in uniaxial tension. In this form, failure will appear once the damage D approaches the value of one.

In this article, the RTCL criterion is used with shell elements. However, void growth is in reality a three-dimensional process. Consequently, in order to model fracture initiation in the best possible way, through-thickness "crack growth" is described as a loss of resistance and stiffness in each through-thickness integration point. The elements are removed once all thickness integration points satisfy the following condition $D > D_{cr}$. The correctness of introducing "through-thickness cracks" by this method may be discussed. After all, shells describe a plane stress situation. Consequently, through-thickness "crack tip" constraints are left out. A more detailed description and investigation of the RTCL criterion is given by Törnqvist [3].

2.2. The BWH instability criterion

Fracture in sheet metal is often preceded by excessive plastic flow in narrow bands, characterized as local necks. Although, the material does not separate immediately, the event of local necking is severe. This is because a significant weakness appears in the material which is quickly followed by fracture.

In accidental analysis of large-scale shell structures, it may be well worth considering the onset of local necking as a state of failure, rather than searching for fracture after local necking has occurred. The reasons for this are twofold. First, the evolution of the local neck cannot be followed with coarse shell elements. This includes the strain state as well as the stress state. In fact, Atkins [24] has reported significant changes in material stress states once local necking appears. Also this effect cannot be captured by large elements. Finally, in the simplest form, the onset of instability can be determined analytically, based on the shape of the material stress–strain curve. This simplifies calibration and yields a pragmatic approach which is appreciated in engineering.

The BWH criterion, [2], gives a simplified way of determining the onset of local necking. It describes an analytical forming limit curve in the stress space, and is therefore not limited to proportional strain paths. The philosophy behind stress based forming limit curves has been convincingly discussed by Stoughton [25,26] and Stoughton and Zhu [27]. The BWH instability criterion combines Hill's local necking analysis [28], with the Bressan and Williams [29] shear stress criterion. In its original form, Hill's criterion assumes that a local neck will form with an angle ϕ to the major principal stress direction. Within the neck, the strain increments along the narrow necking band will be zero. Consequently,

the cross section of the neck will be subjected to plane straining. The orientation of the local neck may be expressed as

$$\phi = \tan^{-1}\left(\sqrt{-1/\beta}\right) \tag{3}$$

where β describes the degree of biaxial straining, $\beta = \dot{\varepsilon}_2/\dot{\varepsilon}_1$, and $\dot{\varepsilon}_1$ and $\dot{\varepsilon}_2$ are the major and minor principal strain rates, see Fig. 1. This yields rational results of ϕ only for negative values of β. It is worth noticing that there is a direct relationship between the stress triaxiality T and β. For the plane stress condition when elastic strains are neglected this yields

$$T = \frac{1}{\sqrt{3}}\frac{\beta+1}{\sqrt{\beta^2+\beta+1}} \tag{4}$$

At the instant a local neck is formed, the effects from strain hardening and the diminution in thickness balance each other exactly. This means that the tractions within the material reach a maximum value at the point of local necking. From these assumptions the following condition for local necking in metal sheets may be derived

$$\frac{\dot{\sigma}_1}{\dot{\varepsilon}_1} = \sigma_1(1+\beta) \tag{5}$$

where σ_1 and $\dot{\sigma}_1$ are the major principal stress and stress rate. Assuming power law plasticity, and that the stress rate ratio $\dot{\sigma}_2/\dot{\sigma}_1$ at the point of instability equals the stress ratio σ_2/σ_1, the following expression for Hill's criterion emerges

$$\sigma_1 = \frac{2K}{\sqrt{3}}\frac{1+\frac{1}{2}\beta}{\sqrt{\beta^2+\beta+1}}\left(\frac{2}{\sqrt{3}}\frac{\tilde{n}}{1+\beta}\sqrt{\beta^2+\beta+1}\right)^n \tag{6}$$

where (K, n) are power law parameters, see Eq. (13). Stoughton and Zhu [27] have presented a similar stress based Hill formulation. The parameter $\tilde{n}$ also represents the power law exponent n, but is indicated differently for practical reasons, see Section 5.1.

According to Eq. (3), Hill's analysis is only valid for negative values of β. In the positive regime, the Bressan–Williams shear stress instability criterion is used. It states that the instability in a sheet element is initiated once a critical shear stress is reached in a direction inclined through the thickness at which the material element experiences no change in length, see Fig. 2.

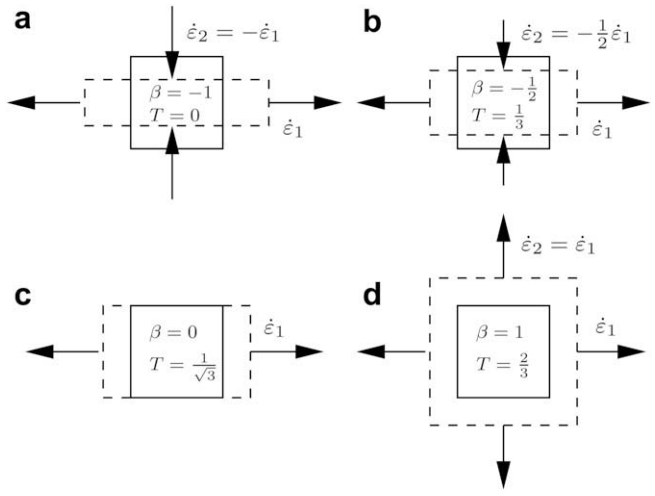

Fig. 1. Strain states in terms of β and T. All conditions refer to stress states for a plane stress element (a) shows a pure shear state, (b) refers to uniaxial tension, (c) illustrates plane straining, and (d) shows equi-biaxial stretching.

This assumption is in fact quite compatible with observations made in Part 1 [1]. In all cases the test components showed inclined failure planes through the thickness. This indicates failure in the direction of the maximum shear stress, as suggested by Bressan and Williams [29]. It is therefore reasonable to assume that this through-thickness shearing instability may take place before any visual signs of local necking. From the detailed derivations given in Refs. [29,2], the following expression for the major principal stress at incipient instability emerges

$$\sigma_1 = \frac{2\tau_{cr}}{\sqrt{1-\left(\frac{\beta}{2+\beta}\right)^2}} \tag{7}$$

where τ_{cr} is the critical shear stress. The Hill criterion and the Bressan–Williams criterion predict failure simultaneously for plane straining ($\beta = 0$) when

$$\tau_{cr} = \frac{1}{\sqrt{3}}K\left(\frac{2}{\sqrt{3}}\tilde{n}\right)^n \tag{8}$$

The following expression is found, [2], by combining the Hill criterion with the Bressan–Williams criterion

$$\sigma_1 = \begin{cases} \dfrac{2K}{\sqrt{3}}\dfrac{1+\frac{1}{2}\beta}{\sqrt{\beta^2+\beta+1}}\left(\dfrac{2}{\sqrt{3}}\dfrac{\tilde{n}}{1+\beta}\sqrt{\beta^2+\beta+1}\right)^n & \text{if } \beta \le 0 \\ \dfrac{2K}{\sqrt{3}}\dfrac{\left(\frac{2}{\sqrt{3}}\tilde{n}\right)^n}{\sqrt{1-\left(\frac{\beta}{2+\beta}\right)^2}} & \text{otherwise} \end{cases} \tag{9}$$

Because the BWH criterion searches for local instability, it applies to membrane stresses and strains only. The effect of bending is left out. When applied in a finite element code, this is achieved by checking failure only in the mid through-thickness integration point of every shell element. Once the criterion is violated, the element is removed and fracture is initiated. Applied in explicit dynamic FE codes it may be useful to allow some additional straining, say 1% additional equivalent strain, before the element is removed. This is to avoid erosion of elements due to stress waves and numerical noise. A more detailed description of the BWH criterion is given in Ref. [2]

2.3. Accounting for element size sensitivity

One major problem with the finite element method is the sensitivity to mesh sizes close to fracture. The effect is apparent in zones with large strain gradients, e.g. close to crack tips, at structural intersections, or in post necking zones. Shell elements are especially sensitive to this effect, due to the plane stress formulation. While the through-thickness stress stabilizes solid elements subjected to thinning, shell elements are only restrained by neighboring elements in terms of in-plane compatibility. Consequently, close to failure, shell elements are free to deform in the thickness direction and may strain excessively in narrow bands as

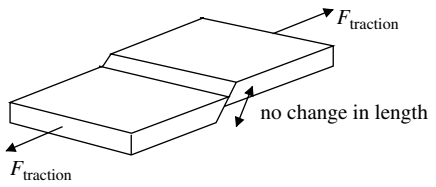

Fig. 2. Illustration of a material element with an inclined through-thickness instability plane. $F_{traction}$ indicate element tractions.

wide as the element itself. This effect is especially seen when small elements are used. When large elements are applied, the problem is rather that strain concentrations remain uncaptured. To minimize this effect, preventive measures are needed.

If small shell elements are used, non-local methods may be applied with success, see Ref. [30]. In this way the damage $\dot{D}$ or strain evolution may be controlled over element boundaries. However, application of non-local methods only makes sense when applied with elements smaller than the sheet thickness. This is due to the fact that the failure mechanisms such as local necking typically take place in narrow bands as wide as the sheet thickness itself, see Ref. [31]. On the other hand, in problems related to collision and grounding of ships, elements with characteristic lengths in the range of 5–15 times the sheet thickness are often used. Obviously, such large elements are unable to detect local instabilities in the material. Several authors have accounted for this discrepancy by making the fracture criterion element size dependent, see for instance Refs. [3,5,32]. Basically, this implies that the failure strain or the critical damage is scaled down to a lower level in order to simulate onset of fracture at the proper resistance level, regardless of the element size.

An engineering correction for the element size effect in shell elements may be derived by considering a deformed material element, see Fig. 3. Assume that a material element strained to the point of fracture consists of two parts. One part contains a local neck with volume V_n, the other part, V_r, is uniformly strained. The sum of V_n and V_r gives the total element volume V_{el}. Assume further that the volume of the developed neck can be followed throughout the process. As plastic incompressibility is assumed, V_n and V_r remain constant during deformation. The average strain at the point of fracture ε_{cr} may now be found from the volume weighted average strain distribution within the material element, see Fig. 3. By applying the average strains ε_n and ε_r for the known volumes V_n and V_r, the critical strain for the total element is given by the following expression

$$\varepsilon_{cr} = \frac{\varepsilon_r V_r + \varepsilon_n V_n}{V_{el}} \tag{10}$$

A similar philosophy is presented by Li et al. [33]. Through rather rigorous derivations, element size effects have been coupled to flaws in the material. The model is referred to as the three-piece-cell model and shows promising results. A further alternative to the is given by Kessler et al. [34]. It follows similar rationale to that presented herein. However, rater than scaling the critical failure strain, focus is placed on evolution of the equivalent strain rate, $\dot{\varepsilon}_{eq}$.

The present expression, Eq. (10), is only valid for shell elements and refers to the elements initial configuration. However, with application in engineering, focus is primarily on a pragmatic scaling law which may operate in an FE code at low cost.

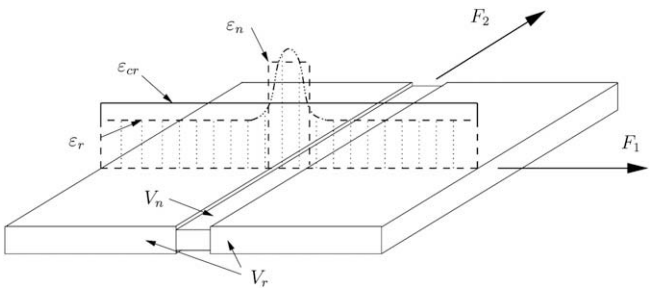

Fig. 3. Simplified illustration of the procedure to generate the critical strain ε_{cr} for a shell element. The constant equivalent critical strain, ε_{cr}, is the volume-weighted result of an assumed element failure strain distribution. ε_r and ε_n indicate the average strain values outside and inside the instability zone, respectively. F_1 and F_2 represent element tractions.

Only equivalent strains are assumed in the following. If the "local neck" forms parallel to the sides of the material element, with an undeformed breadth equal to the initial element thickness t, see Ref. [31], the "instability" volume yields $V_n = t^2 l_e$. This automatically gives the volume of the remaining element, $V_r = V_{el} - V_n = t l_e^2 - t^2 l_e$, where l_e is the undeformed element length. By inserting this into Eq. (10), the following critical strain appears

$$\varepsilon_{cr}(l_e) = \varepsilon_r + (\varepsilon_n - \varepsilon_r)\frac{t}{l_e} \tag{11}$$

This expression is similar to that presented by Lehmann and Peschmann [7], though the basis for the derivation and input values is different.

Calibration of failure criteria may well be done by means of uniaxial tensile tests, as is the case with the RTCL damage criterion. In this case, the formulation of Eq. (11) may be simplified by the following supposition: consider an infinitely long uniaxial tensile test component. If strained to failure, the length of the local and diffuse necking mode will be insignificant compared to the total specimen length. Measured from the crossheads, the specimen would appear to fracture once diffuse necking is reached. This indicates that Eq. (11) converges towards diffuse necking strain as elements become infinity long, e.g. $\varepsilon_{cr}(l_e = \infty) = \varepsilon_r$. Consequently, ε_r takes the value of the diffuse necking strain. Assuming that the material properties can be represented by means of the power law relationship, see Eq. (13), ε_r becomes equal to the power law exponent n. The remaining parameter, ε_n describes the failure strain when $l_e = t$, and can be determined from numerical reproduction of uniaxial tensile tests. For uniaxial tension, Eq. (11), takes the following form

$$\varepsilon_{cr} = n + (\varepsilon_n - n)\frac{t}{l_e} \tag{12}$$

This relation is referred to as a "fracture scaling law" and may be applied directly to calibrate the RTCL criterion Eq. (2), as well as the equivalent strain criterion. It should, however, be mentioned that correcting the failure level as a function of the element size can be dangerous. It is not guaranteed that local deformation mechanisms take part before fracture. Applying methods such as Eq. (12) should therefore be made with caution. Another way to reduce the mesh size sensitivity is to avoid the post-necking zone completely, as exemplified with the BWH instability criterion [2].

3. Modeling the panel indentation tests

Five indentation experiments are described in Part 1 [1]. These have been conducted on 5 mm thick stiffened steel plates, each 1200 mm long and 720 mm wide. The objective behind the tests was to study the deformation response and the resistance to indentation of the panels. The following section reports the finite element modeling and the assumptions which are made.

Table 1
Plate–stiffener configuration.

Specimen	Number of stiffeners	Stiffener type	
US	None	–	
1-FB	One	Flat bar (FB)	120 × 6 mm
1-HP	One	Bulb (HP)	120 × 6 mm
2-FB	Two	Flat bar (FB)	120 × 6 mm
2-HP	Two	Bulb (HP)	120 × 6 mm

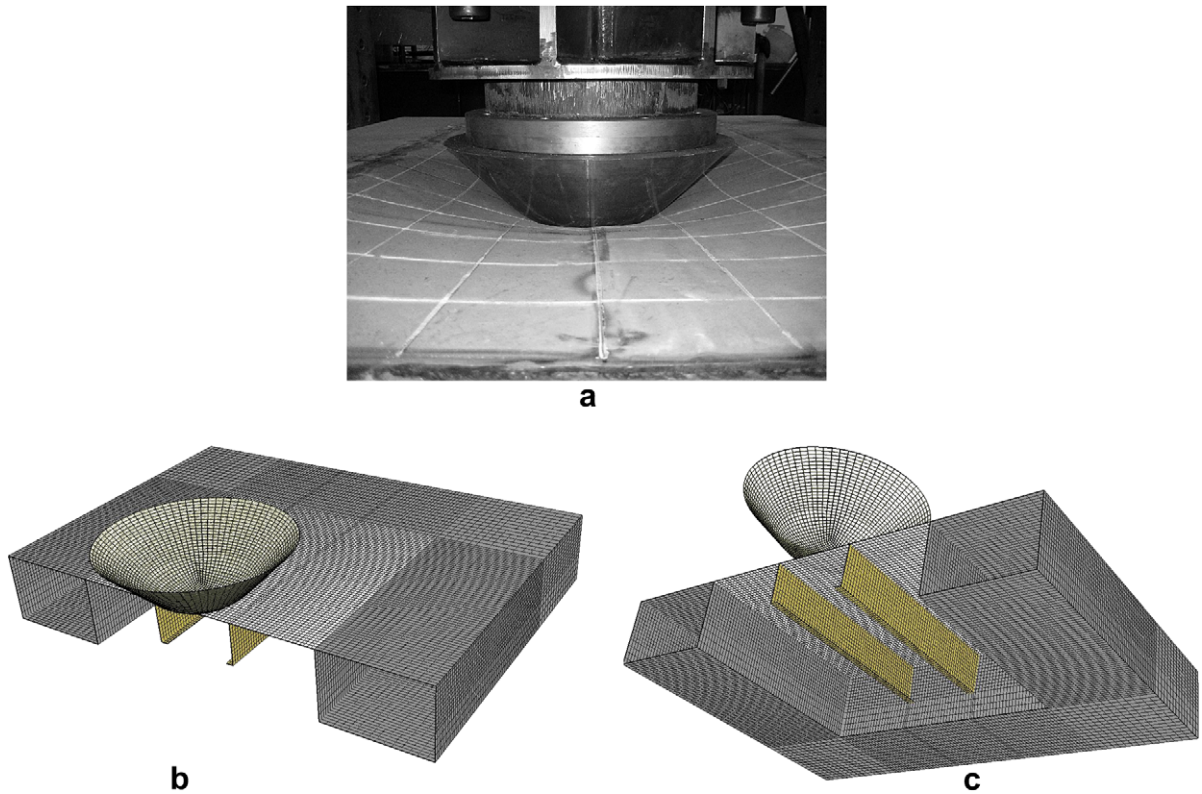

Fig. 4. Illustration of the indentation tests/simulations: (a) shows the indenter and loaded specimen, while (b) and (c) illustrate the upper and lower side of the finite element model of 2-HP, respectively.

3.1. Finite element models

Five indentation tests have been conducted, all with different stiffener configurations. A short description is given in Table 1, see Part I [1] for further details.

The numerical analyses are carried out using the explicit FE code LS-DYNA [21]. Each specimen is modeled using three different characteristic element sizes, $l_e = [5, 10, 18]$ mm, and Belytschko–Lin–Tsay shell elements [35] with five integration points through the thickness. Contact between indenter and plate is accounted for by applying the surface-to-surface contact routines in LS-DYNA. This is enforced with a static friction coefficient equal to 0.3, which is a reasonable assumption for friction between coated steel surfaces. In total 30 simulations have been conducted.

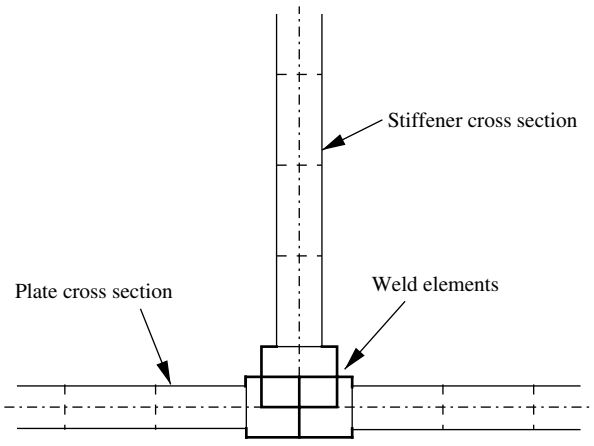

Fig. 5. Cross section illustration of "weld element" in the stiffener–plate junction.

The finite element models are illustrated in Fig. 4. To account for imperfections in the stiffener geometry, a general imperfection in form of a sine curve is applied to the stiffeners. The amplitude of this curve is 0.1% of the stiffener length. Furthermore, it is likely that some offset between the indenter and the target center has been introduced during testing. To account for this, the indenter is set to hit the specimens 5 mm off the panel center.

The additional thickness caused by the weld seams is accounted for by increasing the plate thickness in the plate–stiffener intersection. This is a necessary action, especially when applying small elements, both with respect to the behavior of the stiffeners and to predict the onset of fracture. Adding welds gives an increase in stiffener tripping resistance and a smoother cross-section transition between stiffener and plate. Physically, the weld cross section takes the shape of a triangle. The height and width of the welds vary between 5 and 7 mm. In the simulations, welds are represented by single rows of 6 mm wide elements with increased thicknesses. On the plate side, the thickness increase is equal to 2 mm, and on the stiffener side the thickness increase is equal to 4 mm. A similar procedure for modeling welds is reported by Wang et al. [30]. An illustration is given in Fig. 5.

Table 2
Power law material parameters for the various structural components.

Specimen	Material type	σ_Y [MPa]	K [MPa]	n	ε_{plat}
Plate US, 1-FB and 2-FB	S235JR EN10025	285	740	0.24	–
Plate 1-HP	S235JR EN10025	340	750	0.20	–
Plate 2-HP	S235JR EN10025	260	640	0.22	0.003
Flat bar stiffeners	S235JR EN10025	340	760	0.225	0.015
Bulb stiffeners	S355NH EN10210	390	830	0.18	0.01
Frame	S355NH EN10210	390	830	0.18	0.01

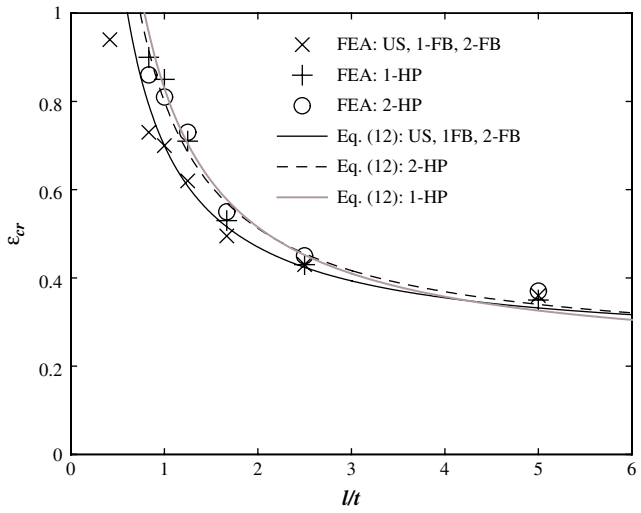

Fig. 6. Equivalent plastic failure strains for different element sizes (uniaxial tension). Data points from FE simulations of tests are compared with curves derived from Eq. (12).

3.2. Material properties

The material is assumed to have isotropic plastic properties and is modeled using plane stress J_2 flow theory. The nominal stress–strain curves for each material sample are given in Part 1, [1]. The equivalent stress–strain relationship is represented by a modified power law formulation which includes the plateau strain.

$$\sigma_{\text{eq}} = \begin{cases} \sigma_{\text{Y}} & \text{if } \varepsilon_{\text{eq}} \leq \varepsilon_{\text{plat}} \\ K(\varepsilon_{\text{eq}} + \varepsilon_0)^n & \text{otherwise} \end{cases} \tag{13}$$

where $\varepsilon_{\text{plat}}$ is the equivalent plastic strain at the plateau exit and σ_{Y} denotes the initial yield stress. The strain ε_0 allows the plateau and power law expression to intersect at $(\varepsilon_{\text{plat}}, \sigma_{\text{Y}})$ and is obtained by

$$\varepsilon_0 = \left(\frac{\sigma_{\text{Y}}}{K}\right)^{\frac{1}{n}} - \varepsilon_{\text{plat}} \tag{14}$$

where K and n are material parameters. The modified power law yields good correlation with the material stress–strain curves, as reported by Alsos et al. [2]. The properties of the materials applied in the experiments are summarized in Table 2.

Material failure is based on the BWH and RTCL criteria, both summarized in Section 2. The BWH criterion is calibrated by the power law exponents given in Table 2, i.e. $\tilde{n} = n$. The critical RTCL damage $D_{\text{cr}}(l_{\text{e}})$ is calibrated from simulations of uniaxial tensile tests with different mesh sizes. This implies that the criterion is made dependent on the mesh size, in order to imitate fracture after onset of local necking. The equivalent strain at fracture is illustrated in terms of the element size in Fig. 6. Here the simulated values are compared with curves produced analytically by Eq. (12). As seen, the correlation is excellent when calibrated values of ε_n are used. For panels US, 1-FB and 2-FB $\varepsilon_n = 0.71$, for plate 1-HP $\varepsilon_n = 0.81$, while $\varepsilon_n = 0.83$ for 2-HP.

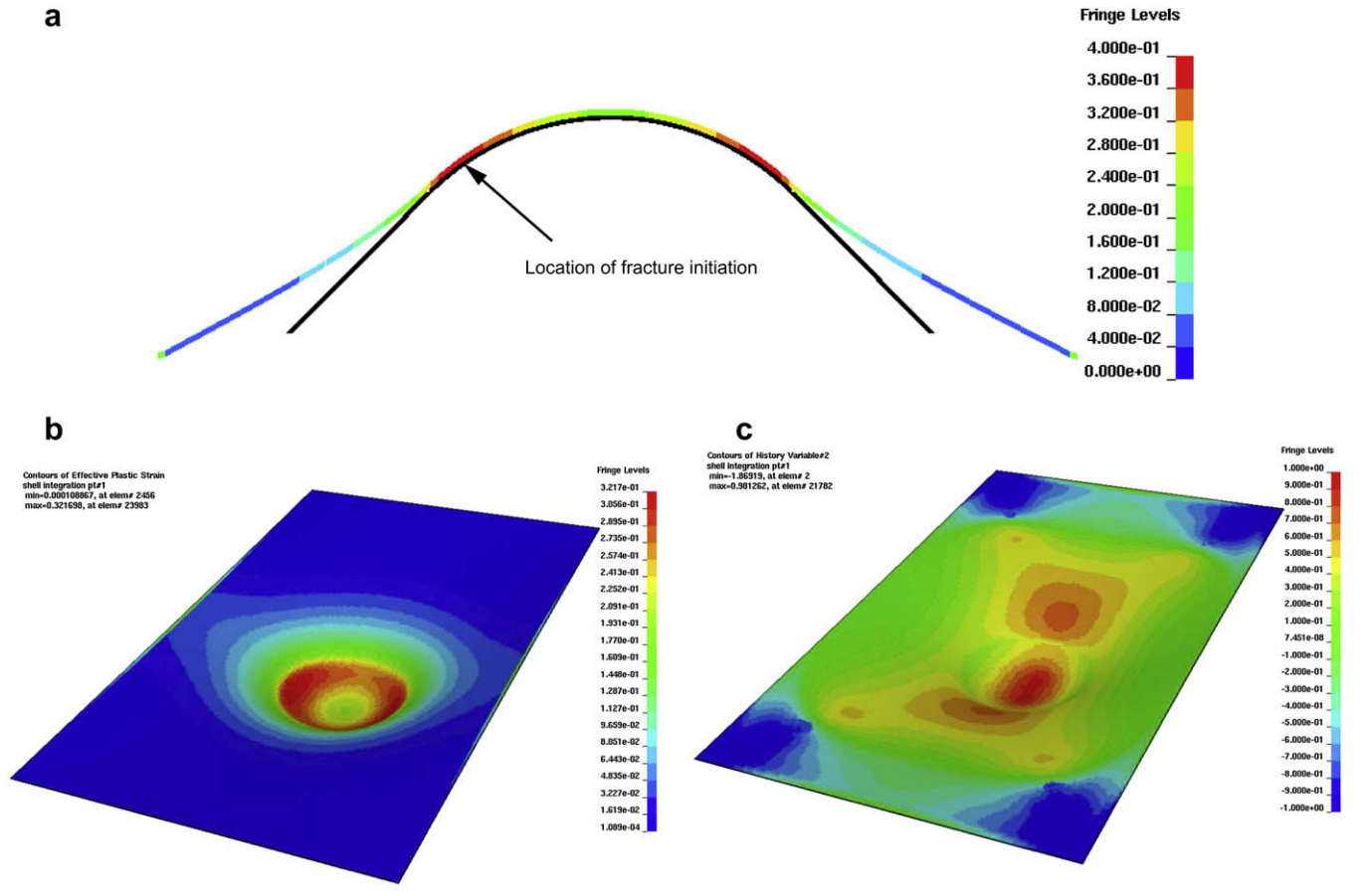

Fig. 7. Indentation of panel US: (a) shows the plastic strain distribution of the transverse cross section of the plate, (b) illustrates the same distribution of the whole plate section and (c) shows the degree of biaxial straining, β, at 175 mm indentation.

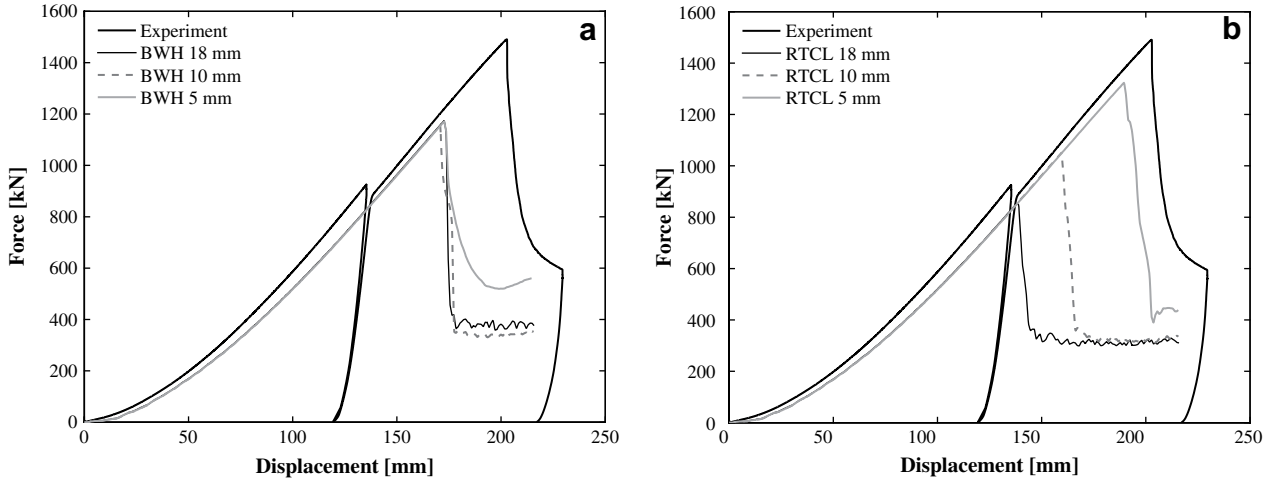

Fig. 8. Force-indentation behavior of panel US: (a) shows simulation results achieved using the BWH criterion, and (b) shows results using the element size dependent RTCL criterion.

4. Simulation results

In this section, the results of the finite element analyses are compared with the experimental results. Focus is placed on the force–deformation relationship and the initiation of fracture.

4.1. Unstiffened plate – panel US

All plates have an aspect ratio close to 5/3. Most of the load is therefore carried in the transverse direction by membrane action. This is seen by analyzing the equivalent plastic strain distribution shown in Fig. 7. The largest strains occur in the plating adjacent to the indenter contact area in the transverse direction. In the direct contact zone deformations are reduced due to friction.

Fig. 7c shows the distribution of strain rate biaxiality β. It is seen that the central impact zone is dominated by equi-biaxial tension, while the most strained areas are dominated by β values closer to 0.3. This corresponds to a loading state between plane strain and equi-biaxial stretching.

The results of the simulations using the two failure criteria are illustrated in Fig. 8. The two criteria show large differences in the failure response. The BWH criterion predicts failure after about 175 mm indentation, irrespective of the mesh size, versus 200 mm in the test.

The RTCL criterion predicts fracture between 120 and 190 mm indentation, depending on the element size. The reason for this is primarily due to the adopted failure scaling law, see Fig. 6. As illustrated in Fig. 7, strain concentrations are weak in the failure zone, though the magnitude of equivalent strain distribution is significant. This correlates well with observations made in Part 1 [1]. Hence, it becomes misleading in this context to implicitly assume local straining and strain concentration effects prior to fracture, as Eq. (12) implies. Simulations performed without damage scaling yields far better correlation with the test, see Fig. 9. In this case, the calibration strain ε_{cr} is set equal to $\varepsilon_n = 0.71$ regardless of the mesh.

4.2. Panels with one stiffener – panel 1-FB and 1-HP

Comparison between simulations and the 1-FB experiment is shown in Fig. 10. The BWH criterion yields excellent results from a resistance point of view, see Fig. 10a. Fracture is predicted between 155 and 160 mm crosshead displacement, versus 175 mm in the test. The RTCL criterion predicts fracture between 130 and 200 mm indentation. Again, the scatter in the RTCL results can be attributed to scaling of the critical damage level, Eq. (12).

The finite element simulations show that the strains in both panels 1-FB and 1-HP are fairly uniformly distributed during deformation. The only exception is when applying the finest element resolution ($l_e = 5$ mm). A narrow strip of elements in the plate close to the stiffener intersection is then observed to strain at a higher rate than the surrounding elements. This is illustrated in Fig. 11a, showing the equivalent plastic strain field (1-FB). These strain concentrations are not detected by the coarser meshes. The location of the onset of fracture will therefore occur at different locations depending on the element size. This is for instance seen in simulations using the BWH criterion. Although the representation of the contact force is excellent for the differently meshed models, the onset of fracture will actually occur at different locations. See for instance Fig. 11. Simulations with the fine mesh shows fracture in the base plate next to the stiffener intersection, as in the tests, while the coarse model fractures about 100–120 mm to the side of the stiffener. In the latter case, strain concentrations are not captured. Hence, the coarsely meshed models show behavior similar to the unstiffened panel.

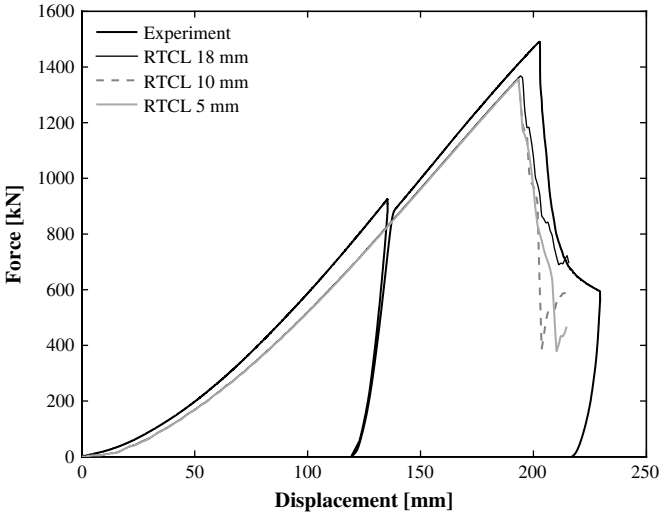

Fig. 9. Force-indentation behavior of panel US. Experimental result compared with simulated results using the RTCL criterion without scaling the critical damage level.

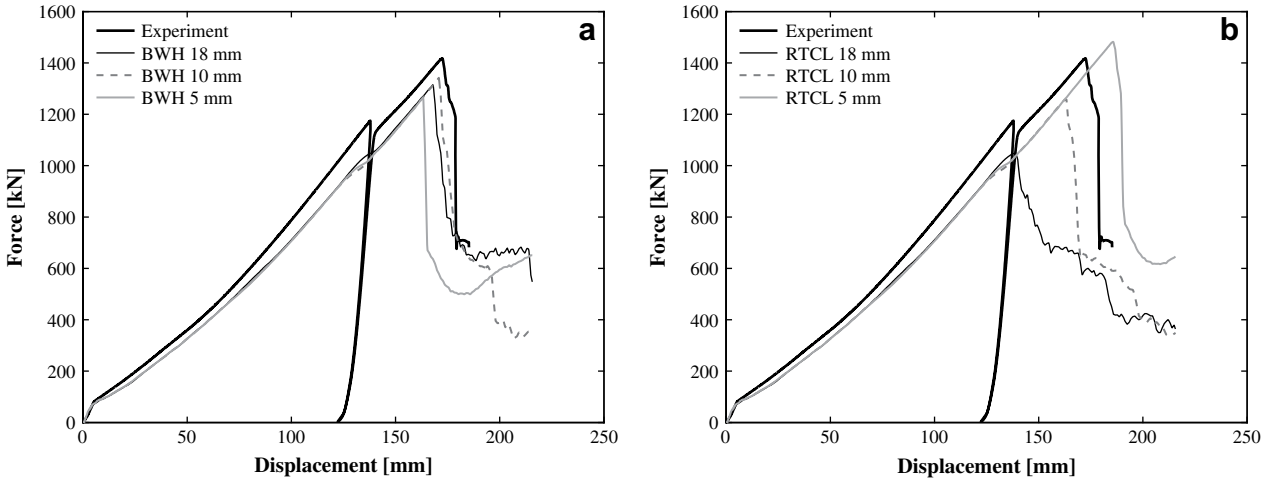

Fig. 10. Force-indentation behavior of panel 1-FB: (a) shows simulation results achieved using the BWH criterion, and (b) shows results using the element size dependent RTCL criterion.

As commented upon earlier, the RTCL results are scattered. Because the mesh scaling law, Eq. (12), fails to separate between locations which in reality are subjected to strain concentrations and areas which are not, fracture initiates prematurely in the uniformly strained areas. Consequently, the coarsely meshed models appear less ductile than FE models having a detailed mesh.

Simulations of 1-HP are in many ways similar to the 1-FB simulations. Again the variations in the RTCL results can be attributed to the "failure scaling law", Eq. (12). The BWH criterion shows more consistent results, though slightly more scattered than for 1-FB, see Fig. 12.

In Part 1 [1], it is observed that once a crack appears it seems to prefer propagating along the weld seam. This results in a sudden loss in transverse membrane capacity. In turn, this leads to a redistribution of the loads in the longitudinal direction. Hence, none of the tests showed a total loss in resistance. The simulations show the same behavior provided that fracture is initiated at the same locations as in the experiments. For this to be the case, a fine mesh is required. Simulations with coarse meshes yield cracks growing in arbitrary directions. The consequence of this is a dramatic drop in resistance, see for instance Fig. 12a.

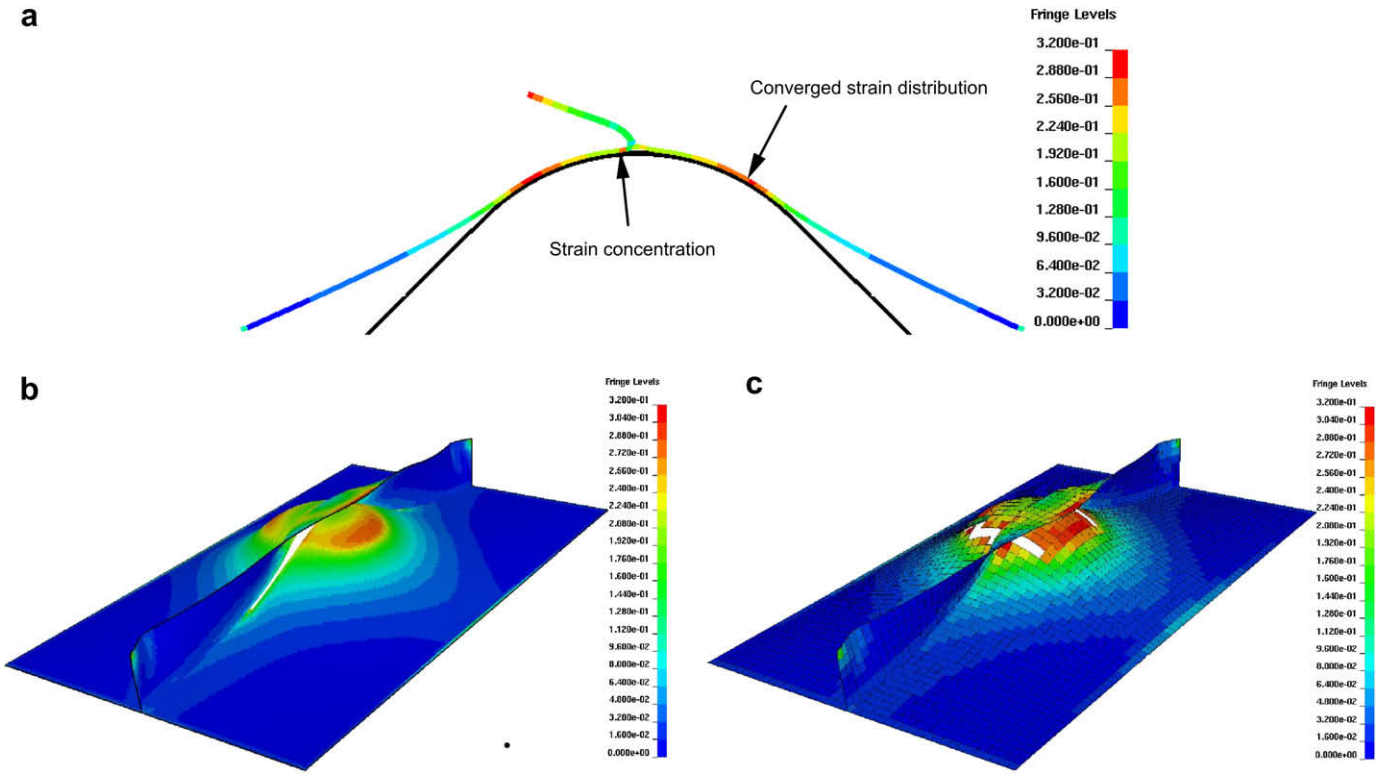

Fig. 11. Deformation of the panels: (a) shows the transverse cross section of panel 1-FB right before fracture, while (b) and (c) illustrate onset of fracture in a fine mesh and a coarse mesh model of 1-FB, respectively. The color distribution illustrates the degree of equivalent plastic straining.

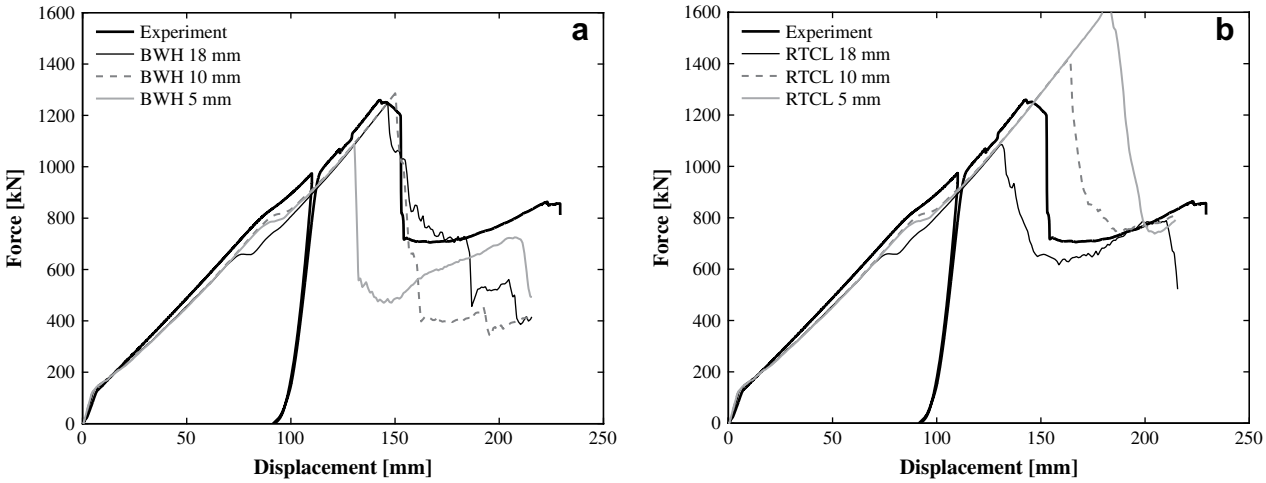

Fig. 12. Force-indentation behavior of panel 1-HP: (a) shows results generated with the BWH criterion, while (b) shows results using the element size dependent RTCL criterion.

4.3. *Panels with two stiffeners – 2-FB and 2-HP*

The simulated indentation of panel 2-FB and 2-HP is depicted in Fig. 13. The plate membrane loads are mainly carried in the transverse direction, through stiffeners and into the frame. As described in Part I, the stiffeners are able to carry significant loads. Consequently, the plate section confined by the stiffeners suffers the most severe deformations. The greatest strains are found in the plate–stiffener intersection. The explanation for this is twofold: first, the combination of large stiffener resistance and friction effects in the impact zone yields greater deformation in the plate section close to the stiffeners than at other locations. Furthermore, the plate–stiffener intersection represents a change in panel geometry, which yields additional strain concentrations. Consequently, fracture occurs at these locations in both 2-FB and 2-HP. This event is simulated successfully with both failure criteria. After the onset of fracture, the crack propagates along the stiffener as monitored in the tests. The discontinuity in the plate caused by the crack reduces the transverse membrane resistance. A consequence of this is that the indenter is wedged in between the stiffeners. This, in turn, accelerates the tripping motion of the stiffeners, which is seen for both 2-FB and 2-HP. The agreement between simulated and

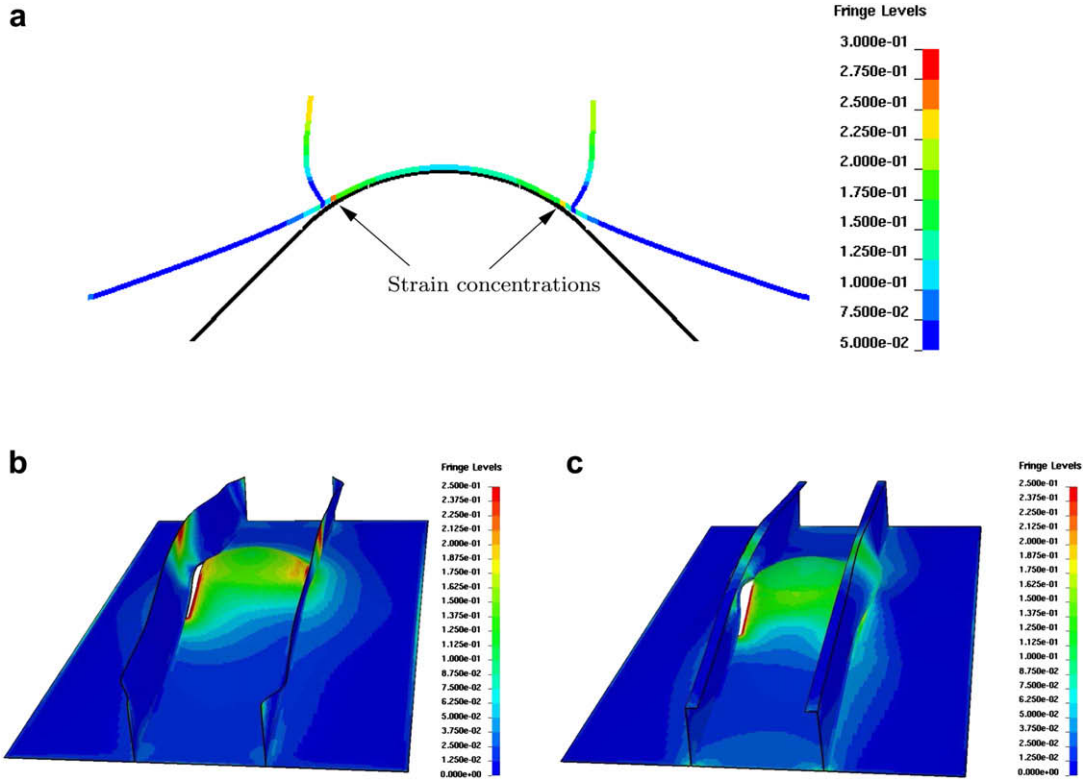

Fig. 13. Deformation of the panels: (a) shows the transverse cross section of panel 2-FB right before fracture, while (b) and (c) illustrate panel 2-FB and panel 2-HP, respectively. The color distribution illustrates the degree of equivalent plastic straining.

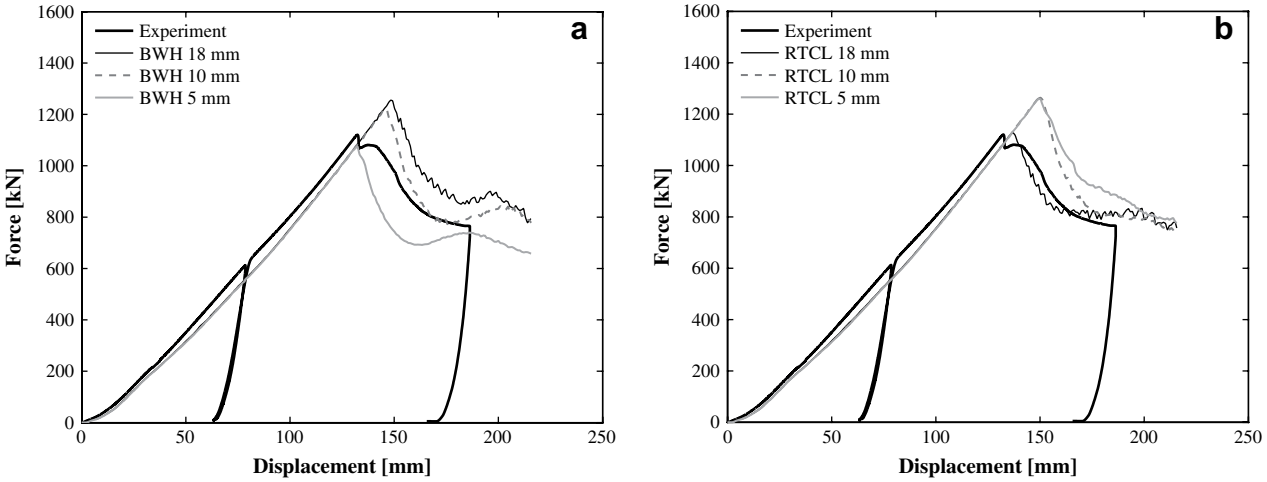

Fig. 14. Force-indentation behavior of panel 2-FB: (a) shows results generated with the BWH criterion, while (b) shows results generated with the scaled RTCL criterion.

experimental deformations is accompanied by an excellent match in force–deformation curves, see Figs. 14 and 15.

Both the BWH and RTCL criteria predict failure with reasonable precision, see Figs. 14 and 15. Scaling the critical damage for the RTCL criterion works well in this case, because fracture is initiated at locations also subjected to dominating strain concentrations, i.e. next to stiffeners. These concentrations are further amplified by bending in the outer and inner surface of the heavily strained row of shell elements next to the stiffeners. Consequently, even though these strain concentrations are not detected by the coarse meshes, they are accounted for implicitly by introducing scaling laws such as Eq. (12).

The BWH criterion shows results with slightly more scatter than those of the RTCL criterion, e.g. penetration of 2-HP in Fig. 15. The BWH criterion applies no element size scaling law. As explained earlier, this is because failure is based on the onset of material instability, rather than the final stage of fracture. Some sensitivity to the element size is, nevertheless, inevitable. Structural intersections and change in geometry yield stress and strain concentrations at large deformations. For coarse meshes this may be difficult to capture. In fact, it may not be possible to capture such strain concentrations correctly or achieve strain convergence at all, even with finer elements. This is due to the plane stress formulation of shell elements, which yield little through-thickness resistance. It is therefore reasonable to assume that extending the element size range will yield an even greater scatter in the force-indentation results if counteractions are not made, e.g. by non-local methods or by corrections such as Eq. (12).

The tests show a remarkable post-failure resistance. For specimen 2-HP, the resistance hardly drops after fracture, Fig. 15. When the plate fractures, the crack path is restricted by the area confined by the stiffeners. The same response is obtained in the simulations with both failure criteria. Because the loads are re-distributed, the effect of crack propagation becomes less significant. This implies that the panel is able to carry significant loads in the longitudinal direction.

5. Discussion

The test results are reproduced well by means of the finite element method. It is demonstrated that onset of fracture may be estimated with good precision, especially when changes in the panel cross section, such as stiffener–plate intersections, are modeled with "weld elements" to give a smoother shell element thickness transition. This is shown in use with the BWH criterion. For the present tests, a significant scatter in the simulation results is observed when applying the RTCL damage criterion in combination with the mesh size dependent failure scaling procedure. This is exemplified in the indentation simulations of specimens US, 1-FB

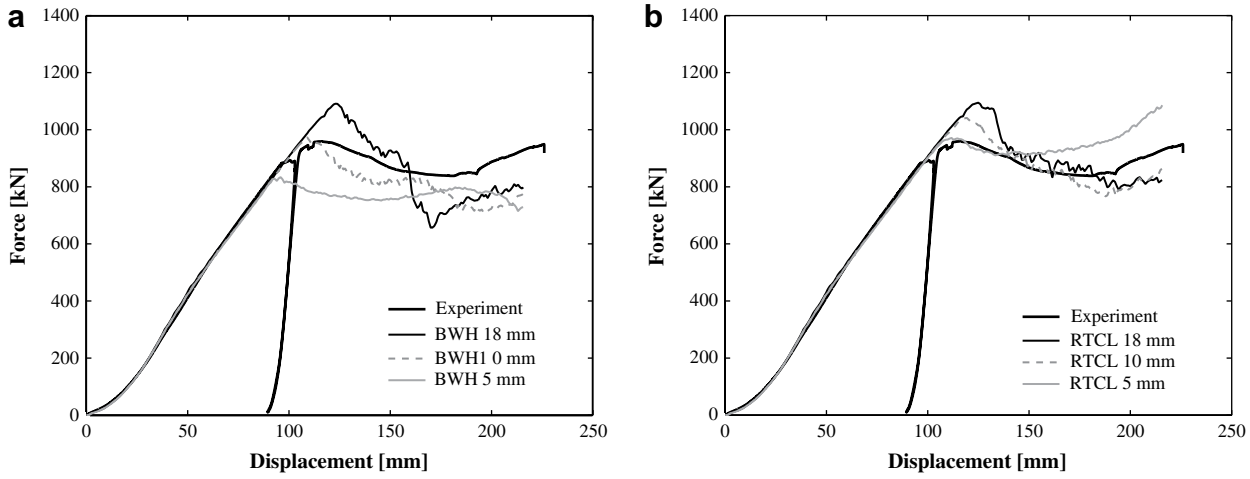

Fig. 15. Force-indentation behavior of panel 1-HP: (a) shows results generated with the BWH criterion, while (b) shows results generated with the scaled RTCL criterion.

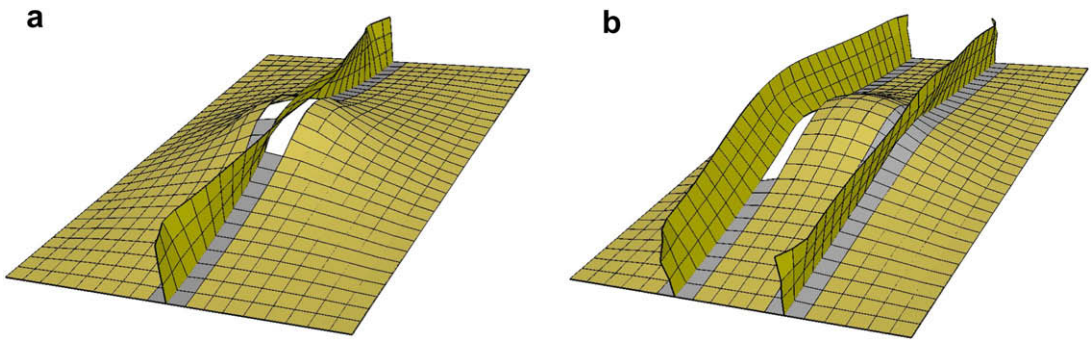

Fig. 16. Simulations of (a) panel 1-FB and (b) specimen 2-FB using the restricted failure scaling law (only gray elements at intersections). The characteristic element size is 8 times the plate thickness.

and 1-HP. However, the problem seems to lie in the way the criterion is scaled rather than in the RTCL criterion itself.

Collision and grounding analysis performed by means of the non-linear finite element method is demanding, mainly because the sheer size of the structure requires large computational resources. A topic often discussed is the element size to be applied in the analysis. Ideally, elements should be capable of capturing the correct failure mechanism. With today's computers, a compromise has to be made in order to complete the analysis with reasonable time consumption. This compromise yields often element sizes in the range of 5–15 times the plate thickness, or more. This is of course not ideal with respect to prediction of fracture. For comparison, the element sizes in the previous simulations, ranged from 1 to 4 times the plate thickness. In the following section, alternative measures to determine fracture in coarsely meshed panels are discussed.

5.1. Alternatives measures

Local necking, fracture and excessive straining usually take place in limited zones. Ideally, it should be sufficient to restrict dense meshes only to these areas. To foresee where such mechanisms will take place is, on the other hand, not trivial, especially in large-scale structures. A promising way to overcome this problem is to initiate re-meshing of elements subjected to excessive straining. This method is referred to as the "adaptive refinement method" and is an option found in several FE codes, e.g. in LS-DYNA [21]. This method, however, also has drawbacks. As shown previously, when dealing with large elements it may be difficult to capture local strain effects. This also indicates that it may be difficult to establish a criterion which restricts mesh refinement to zones which in reality are subjected to strain localizations. For now, such a criterion does not exist. This implies that adaptive re-meshing must be performed prematurely in order to capture strain concentrations, which makes the method computationally expensive.

Accepting that coarse meshes are used extensively, it is perhaps possible to improve the way fracture is introduced. Obviously, scaling the critical failure strain alone has strong limitations. In many cases it is unreasonable to assume local strain fields prior to fracture. Simulations of the unstiffened panel showed for instance no signs of local straining before fracture. Consequently, the use of scaling laws such as Eq. (12) needs restrictions. The simulations carried out in the previous section all showed that strain concentrations appear close to changes in the structural geometry, e.g. plate stiffener intersection and crack tips. It is therefore reasonable to restrict the use of Eq. (12) to locations where strain concentrations most likely will appear, for instance at structural intersections. Enforcing this restriction may be done during pre-processing by running simple programs which read the finite element input file, recognizes all nodes shared by more than four elements (Q4 shell elements), and writes an updated FE input file. In this file, elements at structural intersections have scaled failure properties, refer Eq. (12). The procedure is illustrated in the following.

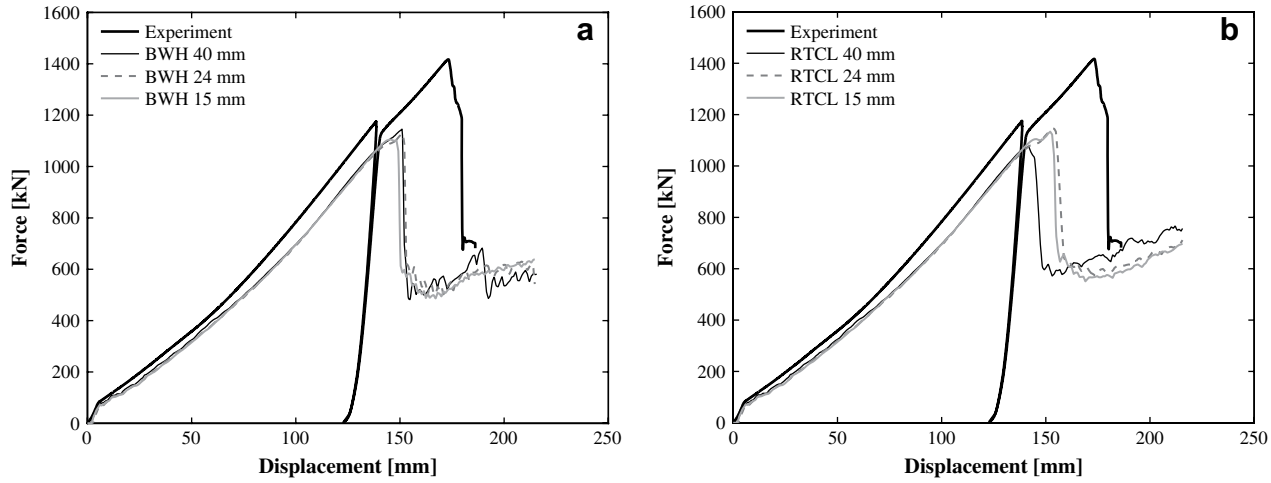

Fig. 17. Force-indentation behavior of panel 1-FB. Failure criterion scaling is used at the plate–stiffener junctions: (a) simulations using the BWH criterion, (b) simulations using the RTCL criterion.

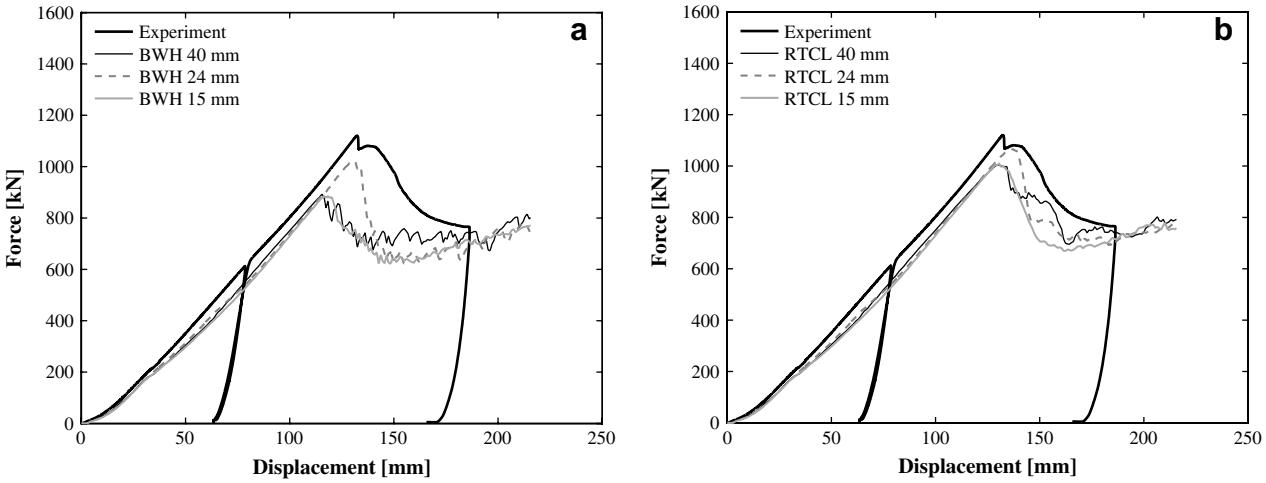

Fig. 18. Force-indentation behavior of panel 2-FB. Failure criterion scaling is used at the plate–stiffener junctions: (a) simulations using the BWH criterion, (b) simulations using the RTCL criterion.

Panels 1-FB and 2-FB are simulated using three additional meshes. The characteristic lengths of the elements are now 40 mm, 25 mm and 15 mm. Since the elements are much larger than the plate–stiffener welds, such details are disregarded. As indicated above, only the elements in the stiffener–plate intersections should have element size dependent properties, Eq. (12). Outside this zone, failure may appear, but no scaling is applied. This rationale may also be used with the BWH criterion. However, this yields a slightly altered expression in zones which are subjected to failure scaling. In this case, the $\tilde{n}$ parameter in Eq. (9) is given element size dependent qualities. According to Hill's analysis the equivalent plastic strain at onset of local necking, in uniaxial tension, is equal to $2n$, refer also Ref. [31]. Inserting this value into Eq. (12) gives the following expression

$$\varepsilon_{cr} = 2\tilde{n} = n\left(\frac{t}{l_e}+1\right) \tag{15}$$

Inserted into the BWH criterion, Eq. (9) can be rewritten as an expression dependent on the element size

$$\sigma_1 = \begin{cases} \dfrac{2K}{\sqrt{3}}\dfrac{1+\frac{1}{2}\beta}{\sqrt{\beta^2+\beta+1}}\left[\dfrac{1}{\sqrt{3}}\dfrac{n\left(\frac{t}{l_e}+1\right)}{1+\beta}\sqrt{\beta^2+\beta+1}\right]^n & \text{if } \beta \le 0 \\ \dfrac{2K}{\sqrt{3}}\dfrac{\left[\frac{1}{\sqrt{3}}n\left(\frac{t}{l_e}+1\right)\right]^n}{\sqrt{1-\left(\frac{\beta}{2+\beta}\right)^2}} & \text{otherwise} \end{cases} \tag{16}$$

As previously, no external input parameters are needed. This approach is intended for elements larger than the sheet thickness itself. For smaller elements, a non-local approach may be preferred.

5.2. Example simulations

Fig. 16 illustrates the indentation and fracture response of 1-FB and 2-FB, respectively. These are simulated using the coarsest mesh ($l_e = 8t$) with the zone restricted "failure scaling law". As expected, fracture now occurs in the plate, next to the stiffeners. This gives a kinematic response which is very similar to the tests.

The force–deformation curves from the simulations are shown in Figs. 17 and 18 and describe the response of 1-FB and 2-FB, respectively. Considering the element sizes used, the results are satisfactory. Some element size effect still exists, as the actual strain field close to the stiffener intersection is not properly captured, but estimated by Eq. (12). This must be expected. After all, this is a simplified way to determine fracture when applying coarse meshes.

6. Concluding remarks

Simulations of the panel indentation tests described in Part 1 [1] have been presented. The five tests are analyzed using different element sizes, introducing "weld elements" and applying two fracture criteria; the BWH instability criterion and the RTCL damage criterion. The results generated with the BWH criterion in general good, although some tendency of mesh sensitivity is present during simulation of the 2-FB and 2-HP models. However, considering the simple implementation and the fact that very few input parameters are needed, the performance of the present criterion is considered to be very satisfactory. Good results may also be achieved using the RTCL criterion, although this requires an increased awareness to input parameters. The RTCL criterion may furthermore be applied with solid elements, while the BWH criterion is restricted to plane stress analysis.

Challenges related to element size effect have been presented. It is shown that this effect varies with structural geometry and load scenario. For instance, when strain gradients do not dominate, the mesh size effect at onset of fracture vanishes. Uncritical scaling of the RTCL damage criterion therefore yields scattered results with respect to prediction of fracture, e.g. as seen in simulations of the US panel. The same is observed in simulations of panels 1-FB and 1-HP. Excellent results are, however, achieved when the RTCL criterion and the scaling law is applied in simulations of 2-FB and 2-HP. In this case, the assumption behind Eq. (12) matches the strain concentrations at the stiffener intersections well. This illustrates the complexity of the problem and shows that the mesh sensitivity problem cannot be treated adequately by means of a fracture-scaling criterion alone.

It is in general recommended to use as small elements as possible. Coarse meshes may have difficulties with capturing strain concentrations. Hence, fracture may be introduced at wrong locations. This may give less accurate results, especially if a failure scaling law is applied uncritically. An alternative method of establishing fracture is therefore presented. This involves restricting the scaling law to apply only at certain locations. For instance, strain concentrations often appear at structural intersections and changes

in plate geometry. Outside these regions, strains usually have smooth distributions. A restriction to the scaling law may therefore be that only elements next to structural intersections or at element crack tips should have scaled fracture properties. Trial simulations performed with coarsely meshed models, which follow this rationale (1-FB and 2-FB), show promising results. Both the failure location and force level corresponds well with the test results. This goes both for simulations with the BWH criterion as well as with simulations performed using the RTCL criterion.

Acknowledgments

The present work is generated as part of the European Community (EC) project "Decision Support System for Ships in Degraded Condition" (DSS_DC). The authors are grateful for the economic support.

References

[1] Alsos HS, Amdahl J. On the resistance to penetration of stiffened plates, part I: experiments. International Journal of Impact Engineering, in press, doi:10.1016/j.ijimpeng.2008.10.005
[2] Alsos HS, Hopperstad OS, Törnqvist R, Amdahl J. Analytical and numerical analysis of local necking using a stress based instability criterion. International Journal of Solids and Structures 2008;45:2042–55.
[3] Törnqvist R. Design of crashworthy ship structures. PhD thesis, DTU; 2003.
[4] Simonsen BC, Törnqvist R. Experimental and numerical modeling of ductile crack propagation in large-scale shell structures. Marine Structures 2004;17:1–27.
[5] Ehlers S, Broekhuijsen J, Alsos HS, Biehl F, Tabri K. Simulating collision response of ship side structures: a failure criteria benchmark study. International Shipbuilding Journal 2008;55:127–44.
[6] Wevers LJ, Vredeveldt AW. Full scale ship collision experiments. TNO-report 98-CMC-R1725. The Netherlands; 1999.
[7] Lehmann E, Peschmann J. Energy absorption by the steel structure of ships in the event of collisions. Marine Structures 2001;15:429–41.
[8] Kitamura O, Kuroiwa T, Kawamoto Y, Kaneko E. A study on the improved tanker structure against collision and grounding damage. In: Proceedings of the seventh international symposium on Practical Design of Ships and Mobile Units (PRADS), den Haag, The Netherlands; 1998.
[9] Naar H, Kujala P, Simonsen BC, Lundolphy H. Comparison of the crashworthiness of various bottom and side structures. Marine Structures 2002;15:443–60.
[10] Simonsen BC, Lauridsen L. Energy absorption and ductile failure in metal sheets under lateral indentation by a sphere. International Journal of Impact Engineering 2000;24:1017–39.
[11] McClintock FA. A criterion for ductile fracture by growth of holes. Journal of Applied Mechanics, Transactions of the ASME 1968;35:363–71.
[12] Rice J, Tracey D. On the ductile enlargement of voids in triaxial stress fields. Journal of the Mechanics and Physics of Solids 1969;17:201–17.
[13] Hancock JW, Mackenzie AC. On the mechanisms of ductile failure in high-strength steels subjected to multi-axial stress-states. Journal of Mechanics and Physics of Solids 1976;24:147–69.
[14] Mackenzie AC, Hancock JW, Brown DK. On the influence of state of stress on ductile failure initiation in high strength steels. Engineering Fracture Mechanics 1977;9:167–88.
[15] Bao Y, Wierzbicki T. On the cut-off value of negative triaxiality for fracture. Engineering Fracture Mechanics 2005;72:1049–69.
[16] Bao Y, Wierzbicki T. A comparative study on various ductile crack formation criteria. Transactions of the ASME 2004;126:314–24.
[17] Bao Y, Wierzbicki T. On fracture locus in the equivalent strain and stress triaxiality space. International Journal of Mechanical Sciences 2004;46:81–98.
[18] Lemaitre J. A continuous damage mechanics model for ductile fracture. Journal of Engineering Materials and Technology, Transactions of the ASME 1985;107:83–9.
[19] Bonora N. Nonlinear CDM model for ductile failure. Engineering Fracture Mechanics 1997;58:11–28.
[20] Wierzbicki T, Bao Y, Lee Y-W, Bai Y. Calibration and evaluation of seven fracture models. International Journal of Mechanical Sciences 2005;47:719–43.
[21] Hallquist J. LS-DYNA theory manual – ls971. Technical report. Livermore, California, USA: Livemore Software; 2007.
[22] Cockcroft MG, Latham DJ. Ductility and the workability of metals. Journal of the Institute of Metals 1968, 96:33–39.
[23] Oh S, Chen CC, Kobayashi S. Ductile failure in axisymmetric extrusion and drawing. Part 2, workability in extrusion and drawing. Journal of Industrial Engineering 1979;101:36–44.
[24] Atkins AG. Fracture in forming. Journal of Materials Processing Technology 1996;56:609–18.
[25] Stoughton TB. A general forming limit criterion for sheet metal forming. International Journal of Mechanical Science 2000;42:1–27.
[26] Stoughton TB. Stress-based forming limits in sheet metal forming. Journal of Engineering Materials and Science 2001;123:417–22.
[27] Stoughton TB, Zhu X. Review of theoretical models of the strain-based FLD and their relevance to the stress-based FLD. International Journal of Plasticity 2004;20:1463–86.
[28] Hill R. On discontinuous plastic states with special reference to localized necking in thin sheets. Journal of Mechanics and Physics of Solids 1952;1:19–30.
[29] Bressan JD, Williams JA. The use of a shear instability criterion to predict local necking in sheet metal deformation. International Journal of Mechanical Sciences 1983;25:155–68.
[30] Wang T, Hopperstad OS, Lademo OG, Larsen PK. Finite element analysis of welded beam-to-column joints in aluminum alloy ENAW 6082 T6. Finite Elements in Analysis and Design 2007;44:1–16.
[31] Hosford WF, Caddell RM. Metal forming, mechanics and metallurgy. 2nd ed. PTR Prentice Hall; 1993. 0-13-588526-4.
[32] Lee Y, Wierzbicki T, Bao Y. Necking, fracture and crack propagation in flat tensile specimens. Report No: 114. Boston, Massachusetts, USA: MIT Impact and Crashworthiness Laboratory; 2004.
[33] Li YN, Karr DG, Wang G. Mesh size effects in simulating ductile fracture of metals. In: 10th international symposium on Practical Design of Ships and other Floating Structures, PRADS. American Bureau of Shipping, ABS. 2007. 0-943870-04-6.
[34] Kessler L, Gese H, Metzmacher G, Werner H. An approach to model sheet failure after onset of localized necking in industrial high strength steel stamping and crash simulations. In: SAE Technical Paper Series No. 2008-01-0503, 2008 World Congress, Detroit, MI: SAE; 2008. 978-0-7680-2003-8.
[35] Belytschko T, Lin JI, Tsay C. Explicit algorithms for the nonlinear dynamics of shells. Computer Methods in Applied Mechanics and Engineering 1984;42:225–51.